4356 *Chem. Mater.* **2010,** *22,* 4356–4363
DOI:10.1021/cm9034159

CHEMISTRY OF MATERIALS
Article

A Layered Titanium Phosphate $Ti_2O_3(H_2PO_4)_2 \cdot 2H_2O$ with Rectangular Morphology: Synthesis, Structure, and Cysteamine Intercalation

László Kőrösi,[†] Szilvia Papp,[†] and Imre Dékány*[,†,‡]

[†]*Supramolecular and Nanostructured Materials Research Group of the Hungarian Academy of Sciences, University of Szeged, H-6720 Szeged, Dóm tér 8, Hungary, and* [‡]*Department of Physical Chemistry and Materials Science, University of Szeged, H-6720 Szeged, Aradi vértanúk tere 1, Hungary*

Received November 9, 2009. Revised Manuscript Received May 23, 2010

Layered titanium phosphate (TiP) composed of rectangular-shaped lamellae was synthesized from titanium isopropoxide and orthophosphoric acid. The as-prepared TiP was refluxed in a 2-propanol/water mixture at ∼363 K for periods up to 144 h. The bulk and surface properties of the lamellar material with novel morphology were studied. The structural investigations and elemental analysis identified TiP as $Ti_2O_3(H_2PO_4)_2 \cdot 2H_2O$. The reactions of the TiP samples with cysteamine (CEA) in aqueous suspensions afforded TiP/CEA intercalation complexes. X-ray measurements on these complexes revealed CEA monolayers incorporated between the TiP lamellae, increasing the original basal spacing from 1.00 nm to 1.43 nm. The enthalpy change of the intercalation reaction was measured by isothermal titration calorimetry. The amount of CEA adsorbed was determined, and differential adsorption enthalpy was calculated via the mass balance.

Introduction

In view of their advantageous properties, the titanium phosphates, which are a group of compounds with highly diverse compositions and structures, are intensively studied in numerous fields, such as ion exchange,[1−3] adsorption,[4] catalysis,[5] etc. They can be utilized as supports[6] or components[7−9] of photocatalysts enhancing the photodegradation of organic molecules. There have been a number of reports on layered,[10] open-framework,[11,12] and mesoporous[13,14] titanium phosphates. Besides their excellent ion exchange capacity, layered titanium phosphates attract considerable interest, because a wide range of organic bases (alkylamines,[15] pyridine,[16] etc.) can intercalate between their lamellae. Such intercalated structures can also be prepared from completely amorphous titanium phosphate. Bortun et al.[17] synthesized such types of semicrystalline materials by reacting propylamine or butylamine with amorphous titanium phosphate, and found that the polymeric (Ti−O−Ti) chains (to which −OH, $-H_2PO_4$, and $=HPO_4$ functional groups are attached) become ordered during the reaction, leading to the formation of a semicrystalline phase with a distinct interlayer distance.

Perhaps one of the best-known layered titanium phosphates is the α-type,[18] characterized by the formula $Ti(HPO_4)_2 \cdot H_2O$, in which the phosphate is present only as HPO_4 groups. In γ-titanium phosphate ($Ti(H_2PO_4)PO_4 \cdot 2H_2O$),[19] there are two different types of phosphates (H_2PO_4 and PO_4). Much less information is available about two further layered titanium phosphates, $TiO(OH)(H_2PO_4) \cdot 2H_2O$[20] and $Ti_2O_3(H_2PO_4)_2 \cdot 2H_2O$.[21] The latter is a novel compound synthesized by phosphoric acid treatment of titanates ($Na_2Ti_3O_7$ and $Na_4Ti_9O_{20}$) at 392−422 K.[22] Takahashi et al.[23] also obtained layered material with the chemical formula $Ti_2O_3(H_2PO_4)_2 \cdot 2H_2O$ (hereafter

*Author to whom correspondence should be addressed. E-mail: i.dekany@chem.u-szeged.hu.

(1) Clearfield, A. *Chem. Rev.* **1988**, *88*, 125.
(2) Bortun, A. I.; Khainakov, S. A.; Bortun, L. N.; Poojary, D. M.; Rodríguez, J.; Garcia, J. R.; Clearfield., A. *Chem. Mater.* **1997**, *9*, 1805.
(3) Airoldi, C.; Nunes, L. M. *Langmuir* **2000**, *16*, 1436.
(4) Maheria, C. K.; Chudasama, U. V. *Ind. Eng. Chem. Res.* **2007**, *46*, 6852.
(5) Clearfield, A.; Thakur, D. S. *Appl. Catal.* **1986**, *26*, 1.
(6) Das, D. P.; Baliarsingh, N.; Parida., K. M. *J. Mol. Catal. A: Chem.* **2007**, *261*, 254.
(7) Kőrösi, L.; Dékány, I. *Colloids Surf., A* **2006**, *280*, 146.
(8) Kőrösi, L.; Papp, S.; Bertóti, I.; Dékány, I. *Chem. Mater.* **2007**, *19*, 4811.
(9) Kőrösi, L.; Oszkó, A.; Galbács, G.; Richardt, A.; Zöllmer, V.; Dékány, I. *Appl. Catal., B* **2007**, *77*, 175.
(10) Clearfield, A.; Roberts, B. D. *Inorg. Chem.* **1988**, *27*, 3237.
(11) Ekambaram, S.; Sevov, S. C. *Angew. Chem., Int. Ed.* **1999**, *38*, 372.
(12) Liu, Y.; Shi, Z.; Zhang, L.; Fu, Y.; Chen, J.; Li, B.; Hua, J.; Pang., W. *Chem. Mater.* **2001**, *13*, 2017.
(13) Jones, D. J.; Aptel, G.; Brandhorst, M.; Jacquin, M.; Jiménez-Jiménez, J.; Jiménez-López, A.; Maireles-Torres, P.; Piwonski, I.; Rodíguez-Castellón, E.; Zajaca, J.; Roziére, J. *J. Mater. Chem.* **2000**, *10*, 1957.
(14) Fei, H.; Zhou, X.; Zhou, H.; Shen, Z.; Sun, P.; Yuan, Z.; Chen, T. *Microporous Mesoporous Mater.* **2007**, *100*, 139.
(15) Espina, A.; Jaimez, E.; Khainakov, S. A.; Trobajo, C.; García, J. R.; Rodríguez, J. *Chem. Mater.* **1998**, *10*, 2490.
(16) Nunes, L. M.; Airoldi, C. *Chem. Mater.* **1999**, *11*, 2069.
(17) Bortun, A.; Strelko, V. V.; Jaimez, E.; García, J. R.; Rodríguez, J. *Chem. Mater.* **1995**, *7*, 249.
(18) Alberti, G.; Cardini-Galli, P.; Costantino, U.; Torracca, E. *J. Inorg. Nucl. Chem.* **1967**, *29*, 571.
(19) Christensen, A. N.; Anderson, E. K.; Andersen, I. G.; Albrti, G.; Nielsen, M.; Lehmann, E. K. *Acta Chem. Scand.* **1990**, *44*, 865.
(20) Li, Y. J.; Whittingham, M. S. *Solid State Ionics* **1993**, *63*, 391.
(21) Bereznitski, Y.; Jaroniec, M.; Bortun, A. I.; Poojary, D. M.; Clearfield, A. *J. Colloid Interface Sci.* **1997**, *191*, 442.
(22) Bortun, A. I.; Bortun, L.; Clearfield, A.; Villa−García, M. A.; García, J. R.; Rodríguez, J. *J. Mater. Res.* **1996**, *11*, 2490.
(23) Takahashi, H.; Oi, T.; Hosoe, M. *J. Mater. Chem.* **2002**, *12*, 2513.

 Published on Web 07/12/2010

designated as TiP) by the reaction of aqueous solutions of titanyl sulfate and ammonium dihydrogen sulfate. The milder reaction conditions (100 °C and relatively low acid concentration) led to the material being less crystalline than that obtained by Bortun et al., even though the chemical formulas of the two substances were identical. To indicate the reduced level of crystallinity, the compound was designated "semicrystalline". Sarkar et al.[24] synthesized new silica-grafted analogs of lamellar TiP under hydrothermal conditions. These modified TiP materials showed good catalytic activity and selectivity in the liquid-phase partial oxidation reactions on a number of substrates.

Reactions between acidic metal(IV) phosphates and various amines or aminothiols are of outstanding importance, because they can be utilized for the synthesis of inorganic/organic hybrid materials with novel characteristics. Cystamine and its reduced form, cysteamine (CEA), which are decarboxylated derivatives of cystine and cysteine, respectively, are biologically important compounds administered as drugs in the therapy of various diseases and against the deleterious effects of ionizing radiation.[25,26] CEA monolayers are frequently applied as linkage layers on Au and Ag surfaces to promote the adsorption of other biomolecules.[27] In this way, enzyme-based biosensors can be constructed through a self-assembly technique.[28] The high affinity of CEA for noble-metal surfaces and metal phosphates is due to its $-SH$ and $-NH_2$ groups, respectively. SH-functionalized titanium phosphates are suitable for the immobilization of Au and Ag nanoparticles, opening the way to the construction of novel supported catalysts or biosensors. Intercalation of compounds containing mercapto groups allows the synthesis of adsorbents of a new type capable of binding toxic heavy-metal ions (Hg^{2+}, Cd^{2+}, Pb^{2+}, and Cr^{3+}).[29]

The present article discusses the structural properties of TiP obtained from titanium(IV) isopropoxide and orthophosphoric acid. The crystallization of as-prepared TiP was studied in refluxing water/2-propanol at atmospheric pressure and ~363 K. The intercalation of CEA into the host material was monitored by X-ray diffraction, thermogravimetry, and titration microcalorimetry. We are not aware of any other report on the calorimetric investigation of CEA intercalation into this TiP compound. Nevertheless, these calorimetric data can contribute to a better understanding of the intercalation process.

Experimental Section

Synthesis of TiP. To a mixture of 6.5 g of titanium isopropoxide (Fluka, Germany) and 13 cm^3 of 2-propanol (Reanal, Hungary), 9.36 g of 85% (w/w) phosphoric acid (Reanal, Hungary) was added in one portion. The instantaneously formed precipitate was homogenized, after the addition of 250 cm^3 of distilled water, by sonication for 5 min, and aged for 24 h. The suspension was next centrifuged at 6000 rpm and the precipitate was redispersed in 250 cm^3 of distilled water and recentrifuged. The latter step was repeated three times. The washed precipitate was suspended in 50 cm^3 of water and lyophilized. The sample was designated TiP_0h.

The above synthesis was repeated several times but with an additional reflux of the aged dispersions for 12, 24, 48, 96, or 144 h at ~363 K. After reflux, the precipitates were likewise washed and lyophilized. The reflux time was included in the designation of the samples, e.g. TiP_12h. Calcination of the samples was carried out for 3 h at 573, 773, 873, or 973 K in air, at a heating rate of 10 K min^{-1}.

Synthesis of CEA-Intercalated TiP. Each of 0.050 g aliquots of TiP_144h were dispersed by sonication in 25 cm^3 of water, followed by the addition of 25 cm^3 of CEA solution, the concentrations of which were set to produce calculated CEA:TiP molar ratios of 0.6, 1.2, 1.8, 2.4, and 3.0. These molar ratios were included in the designation of the samples (e.g., CEA_TiP_0.6). The suspensions were stirred for 12 h and then centrifuged at 6000 rpm. The sediments were dried at 323 K for 12 h.

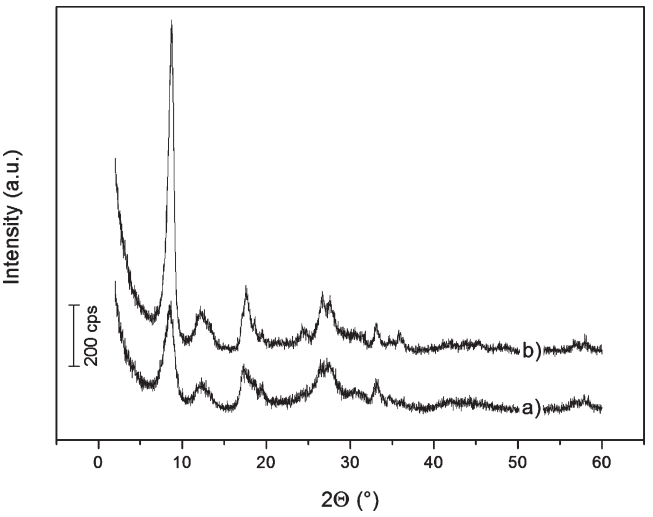

Figure 1. X-ray diffraction (XRD) patterns of (a) TiP_0h and (b) TiP_144h.

Table 1. Effects of Refluxing Time on Crystal Structure of TiP[a]

sample ID	d_{001} peak area[b] (au)	d_{001} position[b] (nm)	D[c] (nm)	N[d]
TiP_0h	684	1.02	7.6	7
TiP_12h	960	1.01	9.4	9
TiP_24h	1094	1.01	11.4	11
TiP_48h	1054	1.01	11.3	11
TiP_96h	1134	1.00	12.9	13
TiP_144h	1181	1.00	13.7	14

[a] Legend: d_{001} = interlamellar distance; D = average crystallite diameter; N = number of individual lamellae within the lamellar stacks. [b] Determined from XRD patterns. [c] Determined using the Scherrer equation from the full width at half maximum (fwhm) of the d_{001} peak. [d] Calculated using the formula $N = D/d_{001}$.

Methods

CEA Adsorption on TiP. Adsorption experiments were performed by a batch method in which 10 mg of the TiP_144h sample was suspended in 10.0 cm^3 of CEA aqueous solution. The CEA concentration of the suspensions was varied in the range of 1.6−12.7 mmol dm^{-3}. The suspensions containing

(24) Sarkar, K.; Nandi, M.; Bhaumik, A. *Appl. Catal., A* **2008**, *343*, 55.
(25) Tremblay, M. E.; Saint-Pierre, M.; Bourhis, E.; Levesque, D.; Rouillard, C.; Cicchetti, F. *Neurobiol. Aging* **2006**, *27*, 862.
(26) Weiss, J. F.; Landauer, M. R. *Toxicology* **2003**, *189*, 1.
(27) Michota, A.; Kudelski, A.; Bukowska, J. *Surf. Sci.* **2002**, *502*, 214.
(28) Guo, S.; Dong, S. *Trends Anal. Chem.* **2009**, *28*, 96.
(29) Hayashi, A.; Nakayama, H.; Tsuhako, M. *Bull. Chem. Soc. Jpn.* **2002**, *75*, 1991.

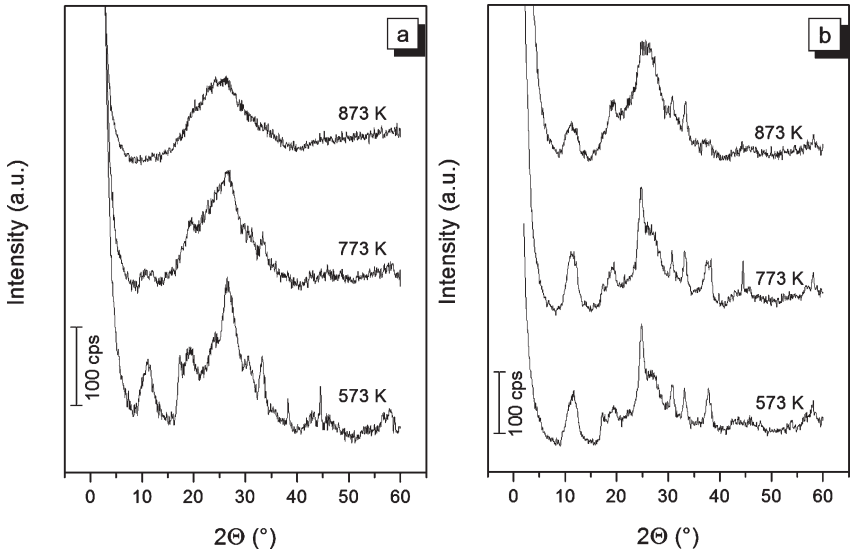

Figure 2. XRD patterns of (a) TiP_0h and (b) TiP_144h after calcination at 573, 773, and 873 K.

various amounts of CEA were stirred at room temperature for 12 h and then centrifuged at 14 500 rpm. Equilibrium CEA concentrations (denoted as c_e (mmol dm^{-3})) were determined by analysis of the total organic carbon (TOC) content of the supernatant of the suspensions. From the initial concentration (c_0 (mmol dm^{-3})) and the volume (V (dm^3)) of the CEA solution, and the mass of the support (m_{TiP} (g)), the amount of CEA adsorbed (n^σ (mmol g^{-1})) can be calculated via the following relationship:

$$n^\sigma = \frac{V}{m}(c_0 - c_e) \quad (1)$$

In the adsorption experiments, the TOC content was measured by means of a Euroglas 1200 TOC Analyzer. The total organic content (TOC) content of the supernatants was varied in the range of 10−300 mg dm^{-3}. The experiment error was within 3%.

The Ti and P contents of the samples were determined by all-argon sequential (Jobin-Yvon 24, France) inductively coupled plasma−atomic emission spectrometry (ICP-AES). The intensities of the (P I) and (Ti II) spectral lines were measured at 213.62 and 337.28 nm, respectively. Before the analysis, weighted samples were dissolved in 48% hydrofluoric acid.

X-ray diffraction patterns were collected on a Bruker D8 Advance diffractometer, using Cu Kα radiation (λ = 0.1542 nm).

Thermogravimetric investigations were conducted in air with a Model TGA/SDTA 851^e (Mettler Toledo) derivatograph at a heating rate of 5 K min^{-1}.

Diffuse reflectance infrared spectroscopy measurements were performed in a Bio-Rad Digilab Division FTS-65A/896 spectrometer, with 256 scans per sample at a resolution of 4 cm^{-1}. The samples (0.008 g) were mixed with dry KBr (0.392 g), and pure dry KBr was used as a reference.

Porosity and surface area were studied on a Model Gemini 2375 (Micromeritics) instrument by recording N_2-sorption isotherms at 77 K. Before the adsorption measurements, the samples were evacuated (1.3×10^{-3} Pa) at 393 K overnight. Specific surface areas were calculated through use of the Brunauer−Emmett−Teller (BET) equation.

Transmission electron microscopy (TEM) images were taken with a Philips Model CM-10 electron microscope, at an accelerating voltage of 100 kV.

Scanning electron microscopy (SEM) was performed with a Hitachi Model S-4700 type cold field-emission instrument equipped with a RönTec QX2 energy-dispersive X-ray spectrometer.

The calorimetric titration experiments were performed at 298 ($\pm 2 \times 10^{-4}$) K, with a thermal activity monitor isothermal heat-flow microcalorimeter (ThermoMetric Model LKB 2277, Lund, Sweden). The sample cell, equipped with a stirring facility and a Lund microtitrator, was loaded with 2.0 cm^3 of a 1.00 g dm^{-3} TiP aqueous suspension. Before titration, the suspension was aged for 1 day. The aqueous solution of CEA (0.5 cm^3, 63.6 mmol dm^{-3}) was injected into the cell in 10 equal steps. The CEA concentration (c_0) was varied from 1.6 mmol dm^{-3} to 12.7 mmol dm^{-3}. The heat effects accompanying adsorption were determined simultaneously in the reference cell, CEA being injected into 2 cm^3 of water. The experiments were performed under constant stirring (60 rpm), and the titrant was injected into the cell at 4 h intervals.

Results and Discussion

Structure and Composition. The diffractograms of TiP_0h and TiP_144h are shown in Figure 1. The peak at 2Θ = 8.78° indicates a layered structure with a basal spacing of d_{001} = 1.00 nm. The intensities of the peaks clearly demonstrate that the crystallinity of TiP_144h is significantly higher than that of TiP_0h. With increasing reflux time, the half-width of the d_{001} peak decreases continuously, indicating an increase in crystallite size (thickness of stacked lamellae). Average crystallite diameters (D) calculated from line broadening according to the Scherrer equation are listed in Table 1. These data reveal that the value of D is about 2-fold higher after reflux for 144 h than in the sample without reflux. Crystallization is also indicated by an increase in the area under the d_{001} peak (Table 1). The calculated quotients of the crystallite diameters and d_{001} values ($N = D/d_{001}$)[30] indicate that the average number of individual lamellae within the lamellar stacks gradually increases from 7 to 14 during crystallization. The diffractograms obtained are in good agreement with those reported by Takahashi et al.[23] for $Ti_2O_3(H_2PO_4)_2 \cdot 2H_2O$.

The P and Ti contents of TiP samples were determined by means of ICP-AES measurements. For each TiP

(30) Szabó, T.; Bakandritos, A.; Tzitzios, V.; Devlin, E.; Petridis, D.; Dékány, I. *J. Phys. Chem. B* **2008**, *112*, 14461.

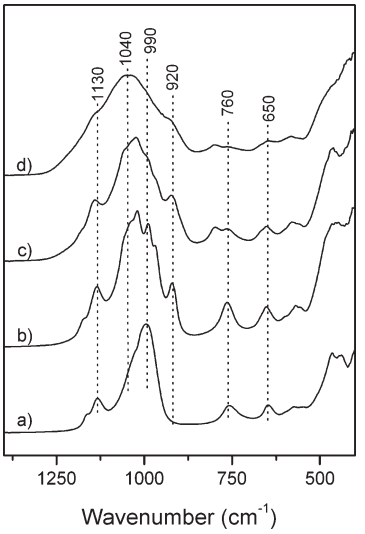

Figure 3. DRIFT spectra of TiP_144h (a) without calcination, or calcined at (b) 573, (c) 773, or (d) 873 K.

powder, the chemical analysis yielded a P:Ti atomic ratio of 1.03 ± 0.025. The measured P and Ti contents of the refluxed samples were 172 ± 4 and 258 ± 2 mg g^{-1}, respectively. These values are in good agreement with those calculated (P: 165.9 mg g^{-1} and Ti: 256.2 mg g^{-1}) for the formula $Ti_2O_3(H_2PO_4)_2 \cdot 2H_2O$. The atomic ratio P:Ti for TiP_0h was also 1.0, but its P and Ti contents were lower than those of the refluxed samples. The difference may be due to the higher content of physisorbed water in the TiP_0h (see TG and N_2-sorption measurements).

The diffractograms of TiP_0h and TiP_144h recorded after calcination at 573, 773, and 873 K are presented in Figures 2a and 2b. The disappearance of the peak at 2Θ = 8.78° after heat treatment at 573 K is characteristic for both samples; this indicates the collapse of the original layered structure. After calcination at 873 K, the sharper reflections in the wide range of angles also disappeared (entirely for TiP_0h but only partially for TiP_144h), and a relatively broad peak was seen in the range of 15°−40°. This means that the high temperature (773−873 K) causes the original structure to collapse and no new crystalline phase is formed. The structural transformation caused by calcination is much more marked for TiP_0h, which is indicative of the higher thermal stability of TiP_144h.

The DRIFT spectra of TiP_144h calcined at various temperatures are compared in Figure 3. The broad band in the range of 920−1230 cm^{-1}, which is characteristic for all these samples, can be assigned to various P−O vibrations. This band broadened after calcination and its maximum shifted from 990 cm^{-1} to 1040 cm^{-1}. Following heat treatment at 573 K, a new band appeared at 920 cm^{-1}; this relates to the asymmetric P−O—P stretching vibrations and is very characteristic of condensed phosphates such as the pyrophosphate group ($P_2O_7^{4-}$).[22,31] The intensity of the band at 760 cm^{-1} assigned to symmetric P−O—P stretching modes, decreased after calcination at 773 K. The band at 650 cm^{-1} is most probably related to the

(31) Lipinska-Kalita, K. E.; Kruger, M. B.; Carlson, S.; Krogh, Andersen, A. M. *Phys. B* **2003**, *337*, 221.

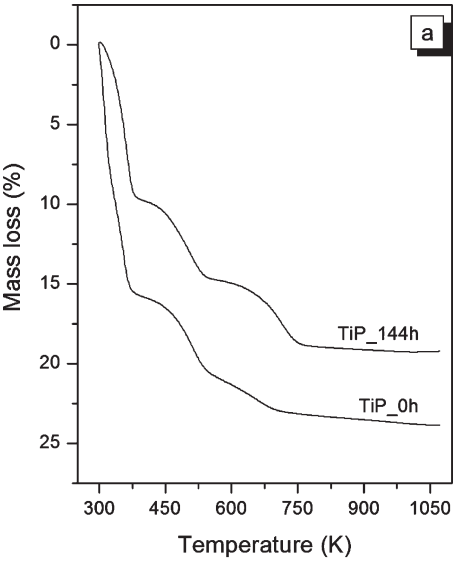

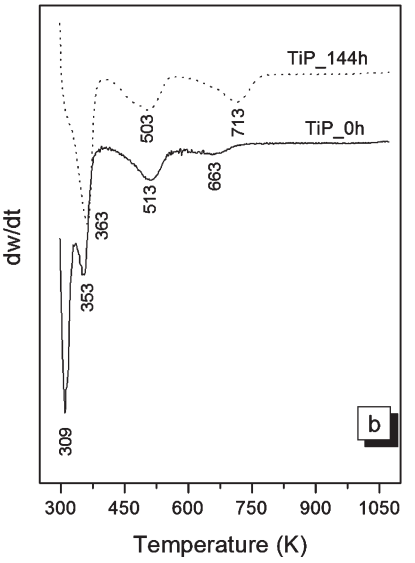

Figure 4. (a) Thermogravimetric (TG) and (b) differential thermogravimetric (DTG) curves of TiP_0h and TiP_144h.

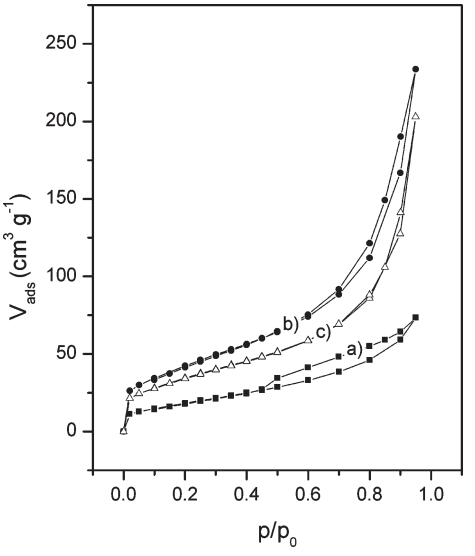

Figure 5. N_2-sorption isotherms of (a) TiP_0h, (b) TiP_12h, and (c) TiP_144h.

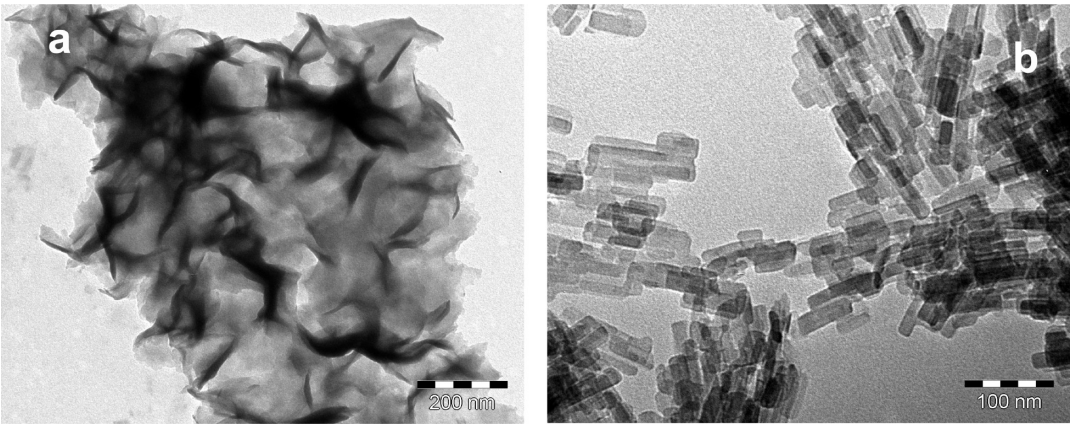

Figure 6. TEM pictures of (a) TiP_0h and (b) TiP_144h.

Ti−O vibration modes of the Ti−O—P framework;[23] its intensity decreased at higher temperatures, just like that of the broad band in the range of 2700−3700 cm^{-1}, which is characteristic of the OH region.

The thermogravimetric curves of TiP_0h and TiP_144h are depicted in Figure 4. The total mass losses from the samples up to 973 K were 23.7% and 19.3%, respectively. The DTG curves (Figure 4b) demonstrate four main stages of mass loss for the sample that was not refluxed, but only three main stages for TiP_144h. The mass loss from TiP_0h between 298 K and 403 K was 15.9%, whereas that from TiP_144h was 9.8%. The larger mass loss from TiP_0h may be due to its different porosity (see the N_2-sorption experiments). Two further mass-loss steps were observed in the ranges of 403−573 K and 573−973 K, with extents of 5.1% and 2.7% for TiP_0h and 5.0% and 4.5% for TiP_144h, respectively. There were no significant differences between the TG curves of the samples refluxed for 12, 24, 48, or 96 h; the differences, with regard to the total mass loss, were $<1\%$.

The data obtained for the refluxed samples agree well with those reported by Bortun et al.,[22] who proposed the formula $Ti_2O_3(H_2PO_4)_2\cdot 2H_2O$ for titanium phosphate synthesized from titanate and phosphoric acid. The thermal changes can be described by the following processes:

$$298-403\ \text{K}: \quad Ti_2O_3(H_2PO_4)_2\cdot 2H_2O \xrightarrow[-2H_2O]{} Ti_2O_3(H_2PO_4)_2 \tag{2}$$

$$403-573\ \text{K}: \quad Ti_2O_3(H_2PO_4)_2 \xrightarrow[-H_2O]{} Ti_2O_3H_2P_2O_7 \tag{3}$$

$$573-973\ \text{K}: \quad Ti_2O_3H_2P_2O_7 \xrightarrow[-H_2O]{} Ti_2O_3(PO_3)_2 \tag{4}$$

Process 3 is confirmed by DRIFT measurements, because the vibrational band characteristic of pyrophosphate appeared after calcination at 573 K. The material was noncrystalline, even after calcination at 873 K; therefore, the formation of condensed phosphates could not be detected by X-ray measurements. In agreement with the X-ray diffractograms, the DTG curve indicated the lower thermal stability of TiP_0h, compared with the refluxed samples, since process 4 finished at a lower temperature. Thus, both the structural studies and the elemental analysis suggest TiP_12h−TiP_144 h are layered titanium phosphates whose chemical formula is $Ti_2O_3(H_2PO_4)_2\cdot 2H_2O$.

There is a significant difference between the N_2-sorption isotherm of TiP_0h and those of the refluxed samples (Figure 5). The hysteresis loop in the isotherm of TiP_0h indicates mesopores, whereas the type II isotherms of TiP_12h−TiP_144 h reflect a flat surface and, in consequence of the absence of hysteresis, a nonporous structure. The porous structure of TiP_0h explains the larger mass loss observed on TG, since a considerable amount of water can be condensed in the pores.

The BET surface areas of the samples after 12, 24, 48, 96, and 144 h of reflux were 157, 146, 135, 129, and 127 $m^2\,g^{-1}$, respectively (i.e., the specific surface area decreased), whereas the crystallinity detected by X-ray measurements increased with increasing reflux time. In view of this observation, it is noteworthy that the surface area of TiP_0h was determined to be only 68 $m^2\,g^{-1}$. This may be due to the lower thermal stability of TiP_0h, which results in a higher degree of collapse during the sample preparation, at the temperature of degassing (393 K).

Morphology. The morphologies of TiP_0h and the refluxed samples are entirely different, as demonstrated by the TEM and SEM pictures (see Figures 6 and 7). TiP_0h consists of wrinkled plates, whereas the refluxed samples formed rectangular lamellae. The SEM pictures of TiP_0h are highly similar to those presented by Wang et al.[32] for lamellar meso-structured TiP, but we have found no reports of rectangular shaped titanium phosphate in the literature. The shorter sides of the projections of the rectangles display a relatively narrow size distribution (15 ± 3 nm), whereas the longer sides measure ~20−150 nm (overlapping interferes with the size determination). The shape of the lamellae did not change upon increasing reflux time.

Cysteamine Intercalation. It is well-known that organic amines can incorporate into layered titanium phosphates. During intercalation, the amine enters the interlamellar space and interacts with the hydrogenphosphate group,

(32) Wang, L.; Yan, Z.; Qiao, S.; Lu, G. Q. M.; Huang, Y. *J. Colloid Interface Sci.* **2007**, *316*, 954.

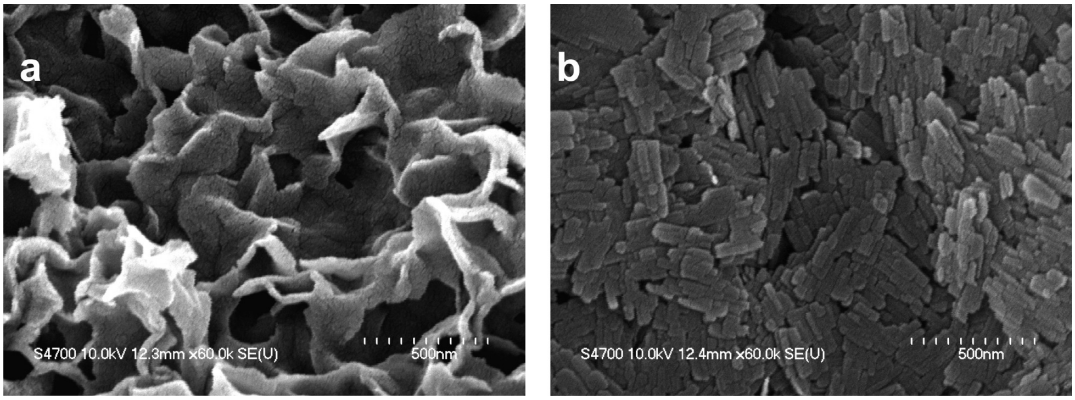

Figure 7. SEM pictures of (a) TiP_0h and (b) TiP_144h.

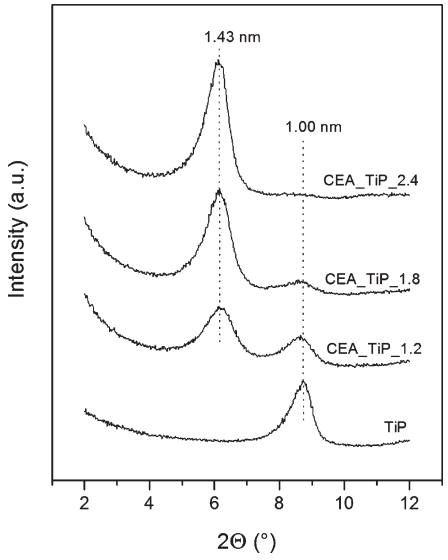

Figure 8. XRD patterns of CEA-intercalated TiP_144h samples.

which can donate a proton to the basic amino group. The organic cations are bound electrostatically to the inorganic lamellae.[33] The incorporation of CEA molecules into the support can be readily followed in the series of diffractograms in Figure 8. In these experiments, the sample with the highest degree of crystallinity, TiP_144h, was used. During CEA intercalation, the intensity of the peak with a *d*-spacing of 1.00 nm gradually decreased and a new peak simultaneously appeared at 1.43 nm. For the intercalation complexes with low amine contents, the phases at 1.43 and 1.00 nm coexist in consequence of the intercalation process not being completed. The peak at 1.00 nm was not observed at all for CEA_TiP_3.0.

The structure of CEA was obtained using the MMFF94 force field[34] by means of implicit solvent model[35] using the Molecular Operating Environment 2007.09 program package.[36] The calculated length of CEA (l_{CEA}) in trans conformation is 0.518 nm. This distance was measured

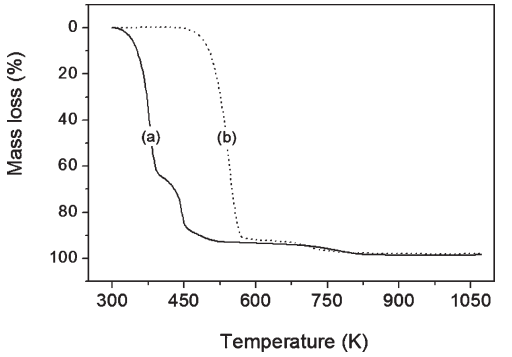

Figure 9. TG curves of (a) CEA and (b) CEA·HCl.

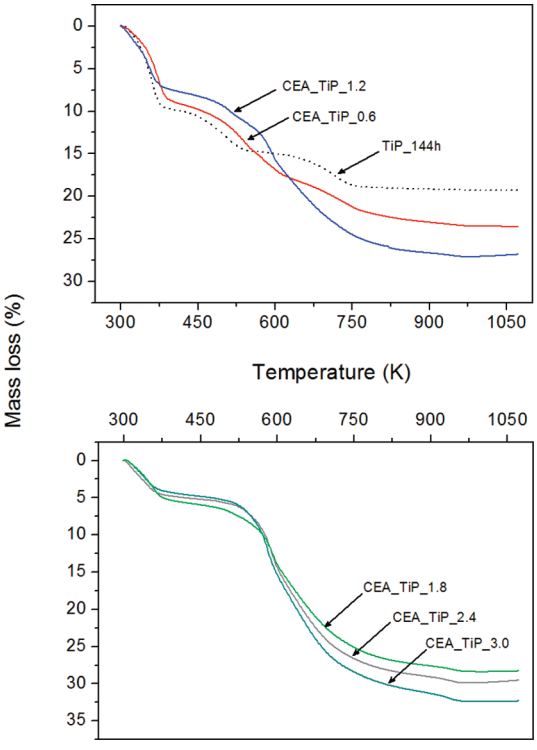

Figure 10. TG curves of CEA-intercalated TiP_144h samples at different CEA:TiP molar ratios.

between the hydrogen atom of —SH group and the mean position of the hydrogen atoms, connected to the nitrogen atom. As the basal spacing of TiP increases by 0.43 nm

(33) Nunes, L. M.; Airoldi, C. *Thermochim. Acta* **2005**, *435*, 118.
(34) Halgren, T. A. *J. Comput. Chem.* **1996**, *17*, 490.
(35) Onufriev, A.; Bashford, D.; Case, D. A. *J. Phys. Chem. B* **2000**, *104*, 3712.
(36) *Molecular Operating Environment* (*MOE 2007.09*): CCG, Montreal, Quebec H3B3X3, Canada.

Table 2. Thermoanalytical Data on CEA-Intercalated TiP_144h Powders and Their Chemical Formulas

sample ID	Mass Loss (%) at 25−130 °C	Mass Loss (%) at 130−700 °C	m_{CEA}[a] (mg g^{-1} sample)	chemical formula at 298 K (determined from TG measurements)
TiP_144h	9.8	9.5	0	$Ti_2O_3(H_2PO_4)_2 \cdot 2.0\ H_2O$
CEA_TiP_0.6	8.9	14.6	51	$Ti_2O_3(H_2PO_4)_2 \cdot 1.8\ H_2O \cdot 0.3\ C_2H_7NS$
CEA_TiP_1.2	7.5	19.6	101	$Ti_2O_3(H_2PO_4)_2 \cdot 1.5\ H_2O \cdot 0.5\ C_2H_7NS$
CEA_TiP_1.8	5.5	22.9	134	$Ti_2O_3(H_2PO_4)_2 \cdot 1.1\ H_2O \cdot 0.7\ C_2H_7NS$
CEA_TiP_2.4	4.9	25.0	155	$Ti_2O_3(H_2PO_4)_2 \cdot 1.0\ H_2O \cdot 0.8\ C_2H_7NS$
CEA_TiP_3.0	4.5	27.8	183	$Ti_2O_3(H_2PO_4)_2 \cdot 0.9\ H_2O \cdot 1.0\ C_2H_7NS$

[a] *m*CEA content of various CEA_TiP intercalation complexes. Value determined from the TG curves in the range of 403−973 K.

during CEA intercalation, it may be concluded that the arrangement in the interlamellar space is monolayer. From eq 5,

$$\sin \alpha = \frac{\Delta d_L}{l_{CEA}} \quad (5)$$

where α is the tilting angle and Δd_L is the difference between the basal spacing values before and after intercalation, the tilting angle of the molecular axis, relative to the lamellar plane, is 56°. For the calculation of α, we suppose that the CEA molecules are in trans conformation in the interlayer space. For γ-titanium phosphate, Hayashi et al.[29] also found that CEA molecules are arranged in a monomolecular layer in the interlamellar space with tilting angle of ~50°.

CEA incorporation was further investigated via thermogravimetric curves. The TG curve of CEA without a support is compared with that of cysteamine hydrochloride (CEA·HCl) in Figure 9. The CEA exhibited a mass loss of 65% up to 403 K, whereas the protonated form was stable up to ~473 K. Comparison of the TG curves for the various CEA_TiP samples (Figure 10) indicates that the height of the first mass loss step (298−403 K) decreases as the CEA:TiP molar ratio increases. This means that the water content of the sample decreases via CEA intercalation. The CEA incorporated among the acidic lamellae is in protonated form, and thus (similar to CEA·HCl, which has higher thermal stability), it is not decomposed up to ~473 K. From these observations, we concluded that only dehydration of the supported samples, but not decomposition of the guest molecule, occurs in the temperature range of 298−403 K. Simultaneously, with processes 2 and 3, the CEA decomposes, and, therefore (as a result of overlapping), only a single step is detected in the temperature range of 403−973 K, especially for samples with relatively high amine contents.

The mass losses from the various samples and the chemical formulas determined from them are reported in Table 2. The above considerations indicated dehydration in the temperature range of 298−403 K. The CEA content (m_{CEA}) was determined from the range 403−973 K; the mass loss of the support in this interval was 9.5%. The composition for the powder with the highest amine content (CEA_TiP_3.0) can be given as $Ti_2O_3(H_2PO_4)_2 \cdot 0.9H_2O \cdot 1.0C_2H_7NS$, i.e. One mole of support binds 1 mol of CEA. The compositions listed in Table 2 demonstrate that, simultaneously with CEA incorporation, the support loses an approximately equimolar amount of water.

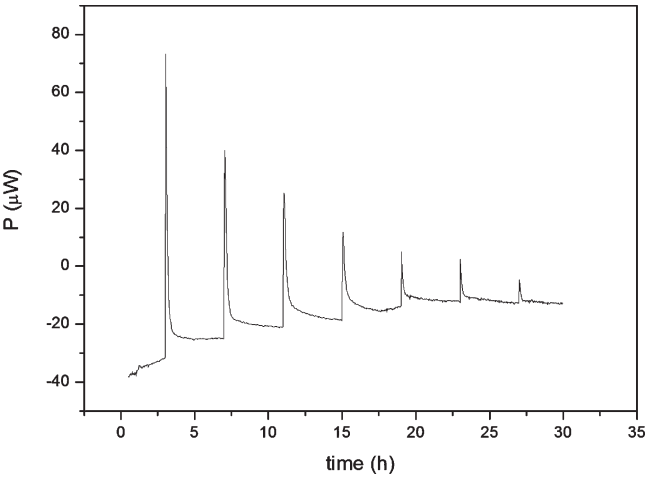

Figure 11. Isothermal titration calorimetric curve of CEA adsorption on TiP_144h.

The adsorption of CEA was also followed by isothermal titration calorimetric measurements. The titration curve showed that the reaction is exothermic (Figure 11). In an aqueous medium, the support is deprotonated (eq 6), and the suspension to be titrated is acidic (pH 4.1). However, the CEA solution is alkaline, as a consequence of the equilibrium depicted in eq 7.

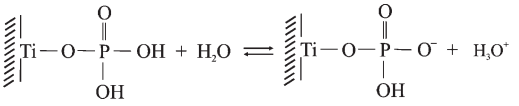

(6)

$$HS-(CH_2)_2-NH_2 + H_2O \rightleftarrows HS-(CH_2)_2-NH_3^+ + OH^- \quad (7)$$

Thus, since an acid is titrated with a base 8, the total enthalpy of reaction (ΔH_{tot}) also includes the enthalpy of neutralization (ΔH^0).

$$H_3O^+ + OH^- \rightleftarrows 2H_2O \quad \Delta H^0 = -57.3\ \text{kJ mol}^{-1} \quad (8)$$

At the first titration point, however, the pH of the medium increases from 4.1 to 7.3, and, thus, the next addition of CEA no longer includes the increment of the enthalpy of neutralization. As demonstrated by the equilibrium described by eq 9, there is an electrostatic

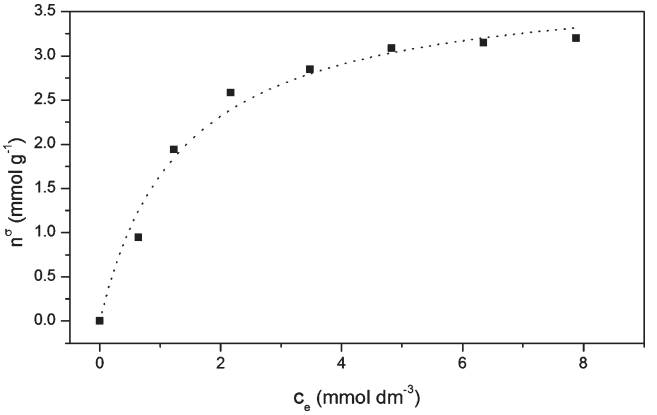

Figure 12. Adsorption isotherm of CEA on TiP_144h at 298 K. The square symbols (■) indicate experimental data, and the dashed line (- - -) represents the Langmuir fit.

interaction between the deprotonated surface and the protonated amine.

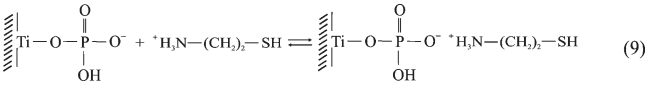

(9)

To calculate the equilibrium concentrations of CEA (c_e) within the calorimeter cell, a Langmuir isotherm (described by eq) was fitted to the (c_e, n^{σ}) data pairs obtained in the adsorption experiments:

$$n^{\sigma} = n^{\sigma}_{max}\left(\frac{Kc_e}{1+Kc_e}\right) \quad (10)$$

where n^{σ}_{max} is the maximum adsorbed amount and K is the equilibrium constant. The nonlinear curve fit (using the Langmuir equation) for the $c_e - n^{\sigma}$ data pairs was performed with Origin 7.0 software; the adsorption isotherm is presented in Figure 12. Combination of eqs 1 and 10 yields

$$-KVc_e^2 + (c_0VK - V - n^{\sigma}_{max}Km)c_e + c_0V = 0 \quad (11)$$

Since the values of c_0 and V during the calorimetric titrations were known, and n^{σ}_{max} and K could be determined from the Langmuir equation, c_e and n^{σ} could be calculated via eq 11. From n^{σ} and the heat of the adsorption, the differential adsorption enthalpy ($\Delta_{ads}H_{dif}$) of CEA on TiP could be calculated. The total changes in enthalpy (ΔH_{tot}) at the individual titration points were corrected by the enthalpies of dilution (ΔH_{dil}), and the values obtained were cumulated in each titration point (see Table 3). Because the material balance of the process is available, the integral adsorption enthalpies obtained ($\Delta_{ads}H_{int}$) can be plotted against the amount of CEA adsorbed on a unit mass of support (see Figure 13). The slope of the straight line fitted to the data series obtained in this way is $\Delta_{ads}H_{dif}$, the value of which is -36.9 kJ mol^{-1}. If the first titration point containing the enthalpy of neutralization is not included in the fitting of the straight line, the relationship $\Delta_{ads}H_{dif} = -37$ kJ mol^{-1} holds.

Table 3. Enthalpies of Intercalation of CEA into TiP_144h and the Related Amount Adsorbed (n^{σ})[a]

n^{σ} (mmol g^{-1})	$-\Delta H_{tot}$ (mJ)	$-\Delta H_{dil}$ (mJ)	$-(\Delta H_{tot} - \Delta H_{dil})$ (mJ)	$-\Delta_{ads}H_{int}$ (J g^{-1})
1.07	102	32.0	70.0	35.0
1.87	78.5	20.3	58.2	64.1
2.41	64.2	17.6	46.6	87.4
2.75	42.9	10.7	32.2	103.5
2.98	26.9	8.9	18.0	112.5
3.13	17.4	7.8	9.6	117.3
3.23	6.1	3.5	2.6	118.6

[a] Legend: ΔH_{tot} = the total enthalpy change of adsorption; ΔH_{dil} = enthalpy of dilution; and $\Delta_{ads}H_{int}$ = the integral adsorption enthalpy.

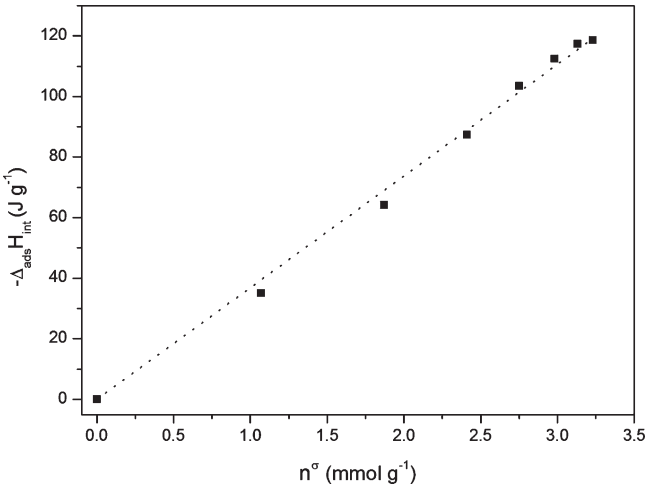

Figure 13. Integral adsorption enthalpies as a function of the amount of CEA adsorbed on TiP_144h.

Conclusion

Titanium phosphate (TiP) with a layered structure was synthesized and identified as $Ti_2O_3(H_2PO_4)_2 \cdot 2H_2O$. The morphology of the as-prepared TiP was found to change completely upon refluxing in a water/2-propanol mixture; the wrinkled plates were transformed to rectangular crystallites. The change in morphology was complete within 12 h; slow crystallization was subsequently observed. After 6 days of refluxing, the average size of the crystallites was 13.7 nm, and their basal spacing was $d_L = 1.00$ nm. TiP prepared without refluxing was mesoporous and macroporous, whereas after crystallization, it had a nonporous structure. In aqueous medium, CEA was spontaneously incorporated into the layered support; the differential adsorption enthalpy was $\Delta_{ads}H_{dif} = -37$ kJ mol^{-1}. The basal spacing in the intercalated powder samples was 1.43 nm; the CEA guest molecules were arranged in a monolayer in the interlamellar space.